Available online at https://sextante-ensb.com

Revista Sextante

ISSN : 2665-3923

Volume: 34 Issue: 01 (2026)

Photocatalytic Degradation of Emerging Organic Pollutants Using Functionalized Semiconductor Nanocomposites

Muhammad Haris*[a], Mah Noor[b], Maryyum Khalid[c]

a. *Corresponding Author: Department of Materials, School of Engineering and Technology, National Textile University, Lahore-Sheikupura Road, Faisalabad-37610 Pakistan (mharis4546@gmail.com)*
b. *Department of Physics, University of Agriculture Faisalabad*
c. *Department of Physics, University of Agriculture Faisalabad*

Article History
Received September 17th, 2026
Accepted November 13, 2026
Published November 24th, 2026

© 2026 The Authors. This article is an Open Access article distributed under the terms and conditions of the Creative Commons Attribution(CC-BY)license https://creativecommons.org/licenses/by/4.0

Abstract
The pervasive contamination of aquatic ecosystems by Contaminants of Emerging Concern (CECs) or Emerging Organic Pollutants (EOPs) including pharmaceuticals, per- and polyfluoroalkyl substances (PFAS), industrial dyes, and microplastics has intensified the demand for sustainable, high-efficiency water remediation technologies. Conventional wastewater treatment plants are largely ineffective at mineralizing these recalcitrant pollutants, while Advanced Oxidation Processes (AOPs), particularly heterogeneously catalyzed solar-driven photocatalysis, offer a promising alternative. This review critically examines the fundamental thermodynamics and kinetics of semiconductor photocatalysis, focusing on energy band energetics, reactive oxygen species (ROS) generation, and Langmuir–Hinshelwood kinetic modeling. It systematically evaluates engineering strategies for functionalized semiconductor nanocomposites, including heterojunction architectures (Type-II, Direct Z-Scheme, and S-Scheme), carbonaceous matrix coupling (biochar, carbon nanotubes, MXenes), metal–organic frameworks (MOFs), and structural lattice tuning via ferroelectric polarization. Degradation pathways and mechanisms are analyzed for key pollutant classes: ciprofloxacin as a pharmaceutical case study, PFOA/PFAS via coupled reductive–oxidative defluorination, and microplastics alongside industrial azo dyes. Performance benchmarks are compared across nanocomposite systems, highlighting trade-offs in redox potential, charge separation, solar utilization, and catalyst stability. Operational challenges including catalyst recovery via magnetic separation, metal ion leaching, matrix interference from inorganic anions and natural organic matter, and continuous-flow reactor design are critically discussed. The review concludes that S-scheme heterojunctions and biochar- or MOF-based composites represent the most promising pathways for scalable, energy-efficient degradation of EOPs, while emphasizing the need for standardized ecotoxicity evaluation and pilot-scale validation under realistic wastewater conditions.

Keywords: Emerging organic pollutants; Semiconductor photocatalysis; S-scheme heterojunction; Reactive oxygen species; Ciprofloxacin degradation; PFAS defluorination; Microplastics; Metal–organic frameworks; Biochar nanocomposites; Advanced oxidation processes

© 2026 The Authors. This article is an Open Access article distributed under the terms and conditions of the Creative Commons Attribution(CC–BY)license
https://creativecommons.org/licenses/by/4.0

1. Introduction

The rapid expansion of global industrialization, intensive agricultural practices, and urbanization has led to the widespread contamination of aquatic ecosystems by Contaminants of Emerging Concern (CECs) or Emerging Organic Pollutants (EOPs) (Richardson & Ternes, 2018). These substances encompass a broad range of chemical classes, including active pharmaceutical ingredients such as ciprofloxacin, tetracycline, sulfamethoxazole, and losartan, fluorinated alkyl substances like perfluorooctanoic acid (PFOA), synthetic textile dyes including Congo Red, Methylene Blue, and Rhodamine B, industrial xenobiotics, and microplastics such as polyethylene, polystyrene, and polyethylene terephthalate (Samal et al., 2022). Furthermore, complex environmental matrices such as landfill leachates introduce shifting concentrations of volatile organic compounds, biochemical oxygen demand (BOD), chemical oxygen demand (COD), and toxic heavy metals depending on the landfill age and waste profile (Kjeldsen et al., 2002).

Conventional municipal and industrial wastewater treatment plants (WWTPs), which rely primarily on mechanical filtration, primary settling, and biological activated sludge processes, are largely ineffective at degrading or mineralizing recalcitrant EOPs. Consequently, these compounds persist through discharge, bioaccumulating in aquatic food webs and posing severe ecotoxicological risks, including endocrine disruption, carcinogenic transformations, and the proliferation of antibiotic-resistant bacteria (Kümmerer, 2009). Secondary treatment alternatives such as physical adsorption onto active matrices or chemical chlorination present significant drawbacks, including phase-transfer limitations without pollutant destruction, high operational costs, multi-step sludge management, and the generation of secondary disinfection byproducts (Ahmed et al., 2017).

Advanced Oxidation Processes (AOPs), particularly heterogeneously catalyzed solar-driven oxidation, represent a sustainable paradigm for point-of-use and industrial water remediation. Heterogeneous photocatalysis utilizes solar light as an energy source to generate reactive oxygen species (ROS) such as hydroxyl radicals (image), superoxide radical anions (image), and singlet oxygen (image) capable of unselectively mineralizing persistent organic structures into non-toxic end products like carbon dioxide (image), water (image), and inorganic mineral acids (Wu et al., 2023).

Despite these advantages, pristine single-component semiconductors such as wide-bandgap titanium dioxide (image) and zinc oxide (image) suffer from critical thermodynamic and kinetic bottlenecks. These limitations include a restricted solar absorption window confined almost entirely to the ultraviolet spectrum (image of total solar irradiance), rapid photoinduced electron-hole (image) recombination kinetics, low surface area, poor chemical stability in extreme aqueous media, and challenges associated with post-treatment catalyst recovery (Hoffmann et al., 1995).

To overcome these constraints, modern chemical engineering strategies focus on the deliberate design of functionalized semiconductor nanocomposites. By integrating tailored functional supports (such as biochar, carbon nanotubes, and metal-organic frameworks), tuning structural lattice morphologies, and constructing anisotropic heterojunction architectures (such as Direct Z-scheme and S-scheme systems), photogenerated charge carrier separation can be spatially enhanced while broadening solar spectrum response into visible and near-infrared (NIR) regimes (Hong et al., 2022).

2. Fundamentals of Semiconductor Photocatalysis and Energy Band Energetics

The fundamental process of heterogeneous photocatalysis is initiated when a semiconductor nanocomposite absorbs incident light photons possessing energy equal to or greater than its bandgap energy ($h\nu \geq E_g$). This optical excitation promotes electrons (e^-) from the occupied Valence Band (VB) across the bandgap to the unoccupied Conduction Band (CB), leaving behind positively charged holes (h^+) in the VB, as shown in Equation 1 (Adewumi et al., 2020):

$$\text{Semiconductor} + h\nu \rightarrow e^-_{CB} + h^+_{VB}$$

The photo-generated e^-_{CB} and h^+_{VB} migrate to the surface of the nanocomposite, where they drive competitive interfacial charge-transfer redox reactions with adsorbed water, hydroxyl ions, dissolved oxygen, or target pollutant molecules. The thermodynamic feasibility of these surface redox reactions is strictly dictated by the absolute energy levels of the semiconductor's CB edge (E_{CB}) and VB edge (E_{VB}) relative to the standard redox potentials of the target species referenced against the Normal Hydrogen Electrode (NHE) (Wright & Kelly, 2017).

To quantitatively predict the electronic band positions of a given functionalized semiconductor material, Mulliken

© 2026 The Authors. This article is an Open Access article distributed under the terms and conditions of the Creative Commons Attribution(CC–BY)license
https://creativecommons.org/licenses/by/4.0

electronegativity theory is broadly applied, as expressed in Equations 2 and 3:

$$E_{VB} = \chi - E_e + 0.5E_g$$

$$E_{CB} = E_{VB} - E_g$$

where χ represents the absolute electronegativity of the semiconductor (defined as the geometric mean of the constituent atomic electronegativities, $\chi = \left[\prod_{i=1}^{n} \chi_i^{a_i}\right]^{1/\sum a_i}$), E_g is the optical bandgap energy, and E_e is the scale-factor energy of a free electron on the hydrogen scale (≈ 4.5 eV vs. NHE). Furthermore, in aqueous media, the flat-band potential shifts as a function of solution pH following Nernstian behavior at 298 K, detailed in Equation 4 (Schneider et al., 2014):

$$E_{\mathrm{pH}} = E^0 - 0.0591 \times \mathrm{pH}$$

For effective pollutant degradation, two main thermodynamic conditions must be satisfied simultaneously:

- **Superoxide Radical Generation**: The E_{CB} potential must be sufficiently negative (more negative than -0.28 V to -0.33 V vs. NHE) to undergo single-electron reduction of dissolved molecular oxygen (O_2) into superoxide radical anions ($O_2 + e^- \rightarrow O_2^{\bullet -}$).
- **Hydroxyl Radical Generation**: The E_{VB} potential must be sufficiently positive (more positive than $+2.27$ V to $+2.38$ V vs. NHE) to oxidize surface-adsorbed H_2O molecules into hydroxyl radicals ($H_2O + h^+ \rightarrow OH^\bullet + H^+$), or more positive than $+1.99$ V vs. NHE to oxidize hydroxide ions ($OH^- + h^+ \rightarrow OH^\bullet$) (Adeoye et al., 2024).

If a semiconductor possesses a narrow bandgap where E_{VB} is less positive than $+1.99$ V vs. NHE (such as zinc indium sulfide, $ZnIn_2S_4$, with $E_{VB} = +1.215$ V vs. NHE), direct oxidation of H_2O or OH^- to $OH^\bullet$ is thermodynamically forbidden. In such cases, the degradation mechanism shifts away from primary VB-driven $OH^\bullet$ production toward indirect ROS formation via $O_2^{\bullet -}$ protonation sequences ($O_2^{\bullet -} + H^+ \rightarrow HO_2^\bullet \rightarrow H_2O_2 \rightarrow OH^\bullet$) or direct hole oxidation of the organic substrate (Adewumi et al., 2020).

The overall reaction kinetics at the solid-liquid interface are frequently modeled using the Langmuir-Hinshelwood heterogeneous catalytic kinetic expression, which integrates target pollutant adsorption equilibria with surface oxidation kinetics. Adsorption isotherms are evaluated using the linearized Langmuir model (Equation 5, assuming monolayer coverage on uniform active sites) or the Freundlich model (Equation 6, assuming multilayer adsorption on heterogeneous energy sites) (Rout et al., 2021):

$$\frac{C_e}{q_e} = \frac{C_e}{Q_0} + \frac{1}{bQ_0}$$

$$\ln q_e = \ln K_f + \frac{1}{n} \ln C_e$$

where C_e ($\mathrm{mg \cdot L^{-1}}$) is the equilibrium pollutant concentration, q_e ($\mathrm{mg \cdot g^{-1}}$) is the amount of pollutant adsorbed per unit mass of nanocomposite, Q_0 and b are Langmuir constants corresponding to maximum adsorption capacity and adsorption energy, respectively, and K_f and n are Freundlich empirical capacity and intensity factors (Hui et al., 2026).

© 2026 The Authors. This article is an Open Access article distributed under the terms and conditions of the Creative Commons Attribution(CC–BY)license
https://creativecommons.org/licenses/by/4.0

3. Engineering Heterojunction Architecture and Functionalization Strategies

3.1 Heterojunction Interfaces: Type-II, Direct Z-Scheme, and S-Scheme Systems

Coupling two or more dissimilar semiconductors with staggered energy band alignments is an effective strategy for suppressing bulk and interfacial e^-/h^+ recombination while maintaining strong redox capabilities. Conventional Type-II heterojunctions inherently sacrifice redox potential because photogenerated electrons migrate to the semiconductor with the less negative CB, and photogenerated holes accumulate on the semiconductor with the less positive VB (Sayed et al., 2026).

To eliminate this thermodynamic sacrifice, Advanced Direct Z-Scheme and Step-Scheme (S-Scheme) heterojunctions have been developed. An S-scheme heterojunction consists of an Oxidation Photocatalyst (OP, having a deep VB and lower Fermi level, E_f) and a Reduction Photocatalyst (RP, having a high CB and higher E_f). Upon intimate physical contact, electrons spontaneously diffuse from RP to OP until their Fermi levels align, generating an Internal Electric Field (IEF) directed from RP to OP at the interface, accompanied by energy band bending (Wang & Shin, 2022).

Under light irradiation, photoexcitation occurs in both components. Driven by the combined action of the interfacial IEF, localized band bending, and Coulombic attraction, the lower-energy photogenerated e^- in the CB of OP recombination-annihilates with the weaker photogenerated h^+ in the VB of RP. Consequently, the most powerful photogenerated e^- remain preserved in the high CB of RP (for strong $O_2^{\bullet-}$ generation), while the most powerful photogenerated h^+ remain preserved in the deep VB of OP (for direct hole oxidation or $OH^{\bullet}$ generation) (Soleimani & Pacchioni, 2025).

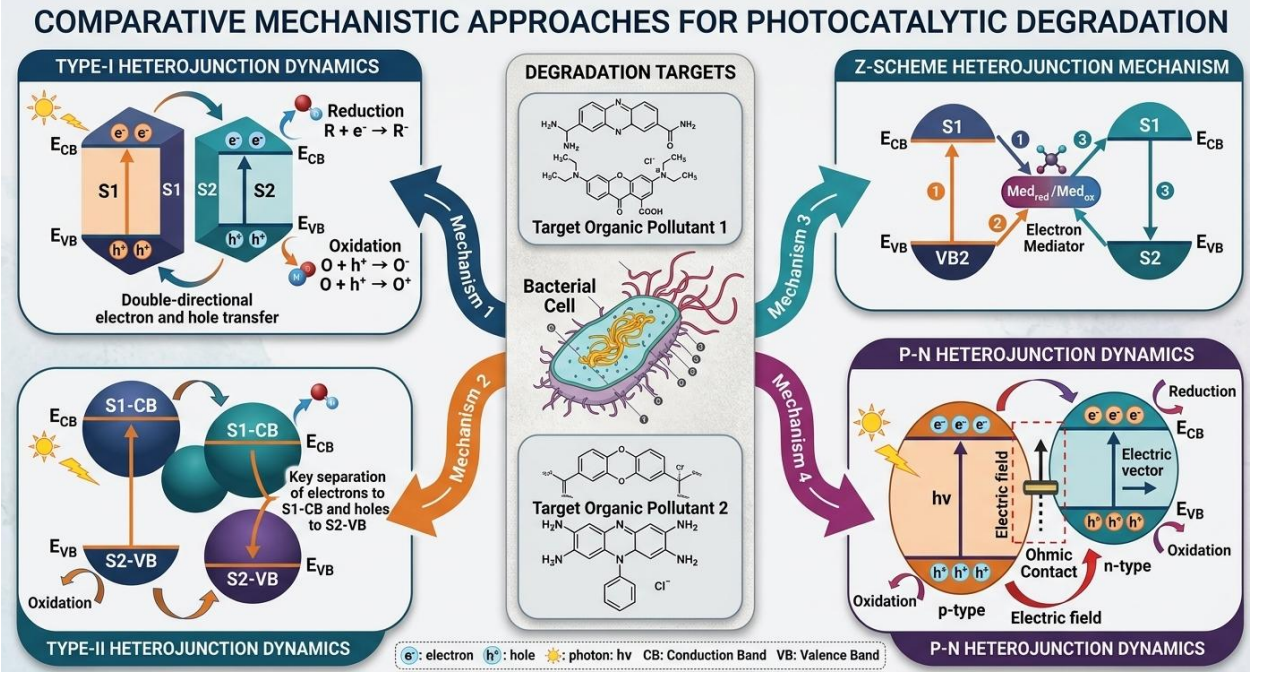


Figure 1: Comparative schematic representation of semiconductor heterojunction dynamics (Type-I, Type-II, Direct Z-Scheme, and P-N heterojunctions) and their interactions with target organic and bacterial pollutants.

© 2026 The Authors. This article is an Open Access article distributed under the terms and conditions of the Creative Commons Attribution(CC–BY)license
https://creativecommons.org/licenses/by/4.0

Table 1. Comparative Mechanics and Energetic Profiles of Heterojunction Architectures

Heterojunction Type	Charge Transfer Direction	Thermodynamic Driving Force	Preserved Reactive Species	Primary Advantages / Limitations
Conventional Type-II	e^- to lower CB; h^+ to higher VB	CB and VB band offsets	Lower redox potential e^- and h^+	Reduced recombination; compromised overall redox overpotential.
Direct Z-Scheme	e^- (lower CB) recombines with h^+ (higher VB)	Interfacial mediator or localized ohmic contact	Powerful e^- (high CB) & h^+ (deep VB)	High redox potential retained; requires precise contact interface geometry.
S-Scheme (Step-Scheme)	Interfacial e^-/h^+ annihilation driven by IEF	Fermi level alignment, IEF, and band bending	Powerful e^- (in RP) & h^+ (in OP)	Spatial charge separation; maximized redox power; optimal solar utilization.

3.2 Functionalization Strategies

3.2.1 Carbonaceous Matrix Coupling

Functionalizing semiconductors with carbon-based nanostructures such as biochar (BC), carbon nanotubes (CNTs), graphene aerogels, and MXenes dramatically improves surface area, pollutant adsorption, and conductivity. Pyrolyzed biochar serves as a high-surface-area support matrix that mitigates nanoparticle aggregation, increasing specific surface area up to three-fold compared to pristine materials (Giannakoudakis et al., 2022). During hydrothermal synthesis or calcination, biochar forms chemical bonds with the semiconductor host, such as covalent Ti-O-C bonds formed by substituting oxygen atoms in the TiO_2 lattice with carbon atoms (Singh et al., 2026). This bond creates localized sub-bandgap electron capture states, narrowing the bandgap energy from 3.20 eV down to 2.63 eV or 1.75 eV, thereby shifting light absorption into the visible spectrum. Furthermore, surface quinone moieties and oxygenated functional groups ($-OH$, $-COOH$, $-COOR$) on the biochar act as electron reservoirs, trapping photogenerated conduction-band electrons and preventing premature recombination (Bellucci, 2026).

In parallel, multi-walled and single-walled carbon nanotubes (CNTs) exploit sp^2-hybridized carbon networks to promote $\pi - \pi$ electron stacking interactions with aromatic contaminants. Functionalizing CNTs with ionic liquids (ILs) converts their native hydrophobic surfaces into hydrophilic interfaces, facilitating uniform dispersion in aqueous media and accelerating interfacial charge transfer kinetics (Kumar et al., 2026).

3.2.2 Metal-Organic Frameworks (MOFs) and Coordination Polymers

Metal-Organic Frameworks (MOFs) including UiO-66 derivatives, ZIF-8, and mixed-linker Ni-MOFs offer high porosity, ultrahigh specific surface areas ($\sim 1000\ m^2 \cdot g^{-1}$), and tunable pore networks. Modifying organic linkers with functional groups such as $-NH_2$, $-OH$, or $-COOH$ alters the energy band edge positions and enhances pollutant adsorption selectivity (Dharsandia et al., 2026).

The operational performance and chemical durability of MOF-based nanocomposites in aqueous environments are governed by the Hard and Soft Acids and Bases (HSAB) principle. High-valence "hard" metal cations (Zr^{4+}, Cr^{3+}, Fe^{3+}) form strong coordination bonds with "hard" carboxylate oxygen donors, yielding high hydrolytic and chemical stability across broad pH ranges. Conversely, softer metal centers combined with weaker organic linkers can suffer lattice collapse and metal ion leaching under dynamic pH or saline conditions. This issue requires structural engineering, such as constructing mixed-linker heterojunctions or encapsulating MOFs within polymeric matrices (Gollavelli & Ling, 2025).

© 2026 The Authors. This article is an Open Access article distributed under the terms and conditions of the Creative Commons Attribution(CC–BY)license
https://creativecommons.org/licenses/by/4.0

3.2.3 Bi-functional and Structural Lattice Tuning

Modifying lattice symmetry, generating intrinsic vacancies, or exploiting internal ferroelectric fields can significantly boost charge separation efficiency. For instance, in strontium niobate ($SrNb_2O_6$) perovskite-like structures, distortion of the NbO_6 octahedra and alignment of the M-O-M bond angle close to 180° creates strong internal ferroelectric polarization fields. This localized electric field drives photogenerated electrons and holes toward opposite crystal facets, suppressing bulk charge recombination (Choe et al., 2026). Additionally, combining semiconductors with bifunctional materials (such as $SrWO_4$, $BiOCl$, or Ag_2S films) enables dual operational capabilities, combining high adsorptive capacity ($> 98\%$ recovery) with efficient visible and near-infrared (NIR) light harvesting (Guan et al., 2025).

4. Degradation Pathways and Mechanisms for Key Emerging Organic Pollutants

4.1 Pharmaceutical Pollutants (Ciprofloxacin Case Study)

The photocatalytic degradation pathways of complex active pharmaceutical ingredients, such as the fluoroquinolone antibiotic ciprofloxacin ($C_{17}H_{18}FN_3O_3$, CIP), demonstrate how targeted ROS attack breaks down complex molecules into harmless inorganic ions. Under solar or visible-light illumination in the presence of functionalized nanocomposites (such as NTP/ZnO-Fe_3O_4, CeO_2-Ag/AgBr, or La/MXene), photogenerated charge carriers yield ROS including $OH^\bullet$, $O_2^{\bullet-}$, and $^1O_2$ (Wan et al., 2025). The relative contributions of these active species are experimentally quantified using selective radical scavenger quenching tests, where isopropanol (IPA) scavenges hydroxyl radicals ($OH^\bullet$), *p*-benzoquinone (BQ) scavenges superoxide radicals ($O_2^{\bullet-}$), and triethylenediamine (TEDA) scavenges singlet oxygen ($^1O_2$) (Yao et al., 2025).

Analytical tracking via high-performance liquid chromatography (HPLC, utilizing symmetrical C18 columns with UV detection at $276\,nm$), 3D fluorescence spectroscopy, and UHPLC-TOF-MS reveals three primary competitive degradation pathways for CIP:

First, piperazine ring cleavage occurs because the piperazine ring contains electron-rich secondary and tertiary amine centers that are highly susceptible to attack by $OH^\bullet$ and $O_2^{\bullet-}$. Oxidative cleavage leads to successive *N*-dealkylation, piperazine ring opening, oxidation to form aldehyde and carboxylic intermediates, and eventual loss of the amine group (Kutuzova et al., 2021).

Second, defluorination and quinolone core substituted hydroxylation proceed through hydroxyl radical attack on the aromatic carbon-fluorine bond ($C\text{-}F$) at the quinolone core. Because fluorine is strongly electronegative, ROS attack induces defluorination, replacing the fluorine atom with a hydroxyl group ($-OH$) to yield hydroxylated non-fluorinated intermediates (Jia et al., 2021).

Third, decarboxylation takes place when ROS attack the carboxylic acid group ($-COOH$) situated on carbon C10 of the quinolone ring. The carboxyl moiety is cleaved, forming intermediate compounds that undergo further ring-opening reactions, ultimately yielding smaller aliphatic carboxylic acids. Continued oxidation breaks these aliphatic fragments down into harmless end products, as described in Equation 7 (Binjhade et al., 2025):

$$C_{17}H_{18}FN_3O_3 + ROS(OH^\bullet, O_2^{\bullet-}, h^+) \rightarrow Intermediates \rightarrow F^- + NO_3^- + CO_2 + H_2O$$

To ensure that photocatalytic degradation reduces overall environmental impact, computational ecotoxicity evaluations using Ecological Structure-Activity Relationships (ECOSAR) predictive modeling are applied. ECOSAR metrics assess acute and chronic toxicity parameters (such as LC_{50} and EC_{50}) across three aquatic trophic levels: fish, *Daphnia*, and green algae. These studies confirm that intermediate transformation products exhibit significantly lower toxicity values than the parent ciprofloxacin molecule, demonstrating the ecological safety of the treatment process (Mukherjee et al., 2021).

© 2026 The Authors. This article is an Open Access article distributed under the terms and conditions of the Creative Commons Attribution(CC–BY)license
https://creativecommons.org/licenses/by/4.0

4.2 Persistent Fluorinated Compounds (PFOA/PFAS)

Perfluorooctanoic acid ($C_7F_{15}COOH$, PFOA) is an extremely persistent environmental pollutant due to the high dissociation energy of its carbon-fluorine bonds (C-F, $\sim 485\ kJ \cdot mol^{-1}$). Pristine photocatalysts generally fail to break down PFOA, but engineered dual-redox semiconductor nanocomposites can achieve efficient defluorination (Yang et al., 2026).

The degradation mechanism follows a coupled reductive-oxidative sequence. Reductive activation is initiated when highly reducing photogenerated conduction-band electrons (e^-_{CB}) directly attack the electron-deficient C-F bonds at the hydrophobic composite interface, weakening the fluorine backbone and initiating initial defluorination. Concurrently, oxidative chain shortening occurs as photogenerated holes (h^+_{VB}) or localized oxygen radicals attack the terminal carboxylic group ($-COOH$), inducing decarboxylation to form a perfluoroalkyl radical ($C_7F^{\bullet}_{15}$) (Liao et al., 2025).

This unstable perfluoroalkyl radical reacts with surface hydroxyl species or water, forming perfluoroalkyl alcohols ($C_7F_{15}OH$) that spontaneously eliminate hydrogen fluoride (HF) to yield shorter-chain perfluorinated carboxylic intermediates ($C_nF_{2n+1}COOH$, where n decreases stepwise from 6 to 1). Repeated cycles lead to complete mineralization into CO_2 and fluoride ions (F^-) (Mehmood et al., 2026).

4.3 Microplastics and Industrial Dyes

Microplastics (MPs) ranging from addition polymers like polyethylene (PE), polypropylene (PP), polystyrene (PS), and polyvinyl chloride (PVC) to condensation polymers like polyethylene terephthalate (PET) and polyurethane (PUR) exhibit varying degradation kinetics based on their chemical bond energies. Non-polar carbon-carbon backbones (C-C) require higher activation energies for cleavage compared to heteroatom-containing linkages such as ester (O-CO), ether (C-O), or aromatic rings (Ioni et al., 2025). Under irradiation, functionalized Z-scheme and S-scheme nanocomposites direct ROS ($O^{\bullet-}_2$, $OH^{\bullet}$) to attack vulnerable heteroatom sites and tertiary carbons in polymer chains. This ROS attack causes chain scission, continuous Norrish-type photo-oxidation, formation of carbonyl and hydroxyl intermediates, and gradual mineralization into non-toxic species (Johannessen & Shetranjiwalla, 2021).

When degrading industrial azo dyes (such as Congo Red or Methylene Blue), partial cleavage of the primary azo linkage ($-N{=}N-$) can initially yield aromatic amines (e.g., benzidine), which are toxic and carcinogenic. Complete mineralization or extended hydraulic retention times are therefore necessary to ensure these toxic intermediates are fully degraded into CO_2, NO^-_3, and SO^{2-}_4 (Hossain, 2024).

5. Performance Benchmark and Kinetic Evaluation of Nanocomposite Systems

To systematically evaluate the performance of functionalized semiconductor nanocomposites across different pollutant classes, key operational parameters including structural composition, target pollutant, light source, primary reactive species, reaction kinetic rate constants (k), and degradation efficiencies are summarized in Table 2.

© 2026 The Authors. This article is an Open Access article distributed under the terms and conditions of the Creative Commons Attribution(CC–BY)license
https://creativecommons.org/licenses/by/4.0

Table 2. Performance Benchmark of Functionalized Semiconductor Nanocomposites for Emerging Organic Pollutant Degradation

Nanocomposite Catalyst System	Target Pollutant Class	Illumination Source	Apparent Kinetic Rate Constant (kkk) / Removal Efficiency	Primary Active Species Involved	Operational Key Features / Stability
g-C_3N_4/ZnO Heterojunction	Pharmaceuticals / Antibiotics	Simulated Visible Light	$> 90\%$ removal efficiency within 60 min	h^+, $O_2^{\bullet-}$ dominant	Z/S-scheme spatial charge separation; high crystallinity.
TiO_2/AC/Fe_3O_4 Magnetic Composite	Industrial Effluent Pollutants	Visible Light	$> 75\%$ efficiency sustained over 5 cycles	$OH^{\bullet}$, h^+, $O_2^{\bullet-}$	Waste-derived bio-carbon; easy magnetic separation.
α-Fe_2O_3/ g-C_3N_4/SiO_2 S-Scheme	Synthetic Dyes (Rhodamine B)	Natural Solar Light	$k = 0.147\ \text{min}^{-1}$ [cite: 25]	$O_2^{\bullet-}$, $OH^{\bullet}$	Enhanced internal reflection & scattering in nanostructure.
ZnCuCr-TpIm MOF Network	Azo Dyes (Congo Red)	Dark Adsorption + Light	87% at pH 8; 64% at pH 10 [cite: 3]	Surface h^+, Direct adsorption	Ultrahigh surface area ($\sim 1000\ \text{m}^2 \cdot \text{g}^{-1}$); Type I isotherm.
La/MXene (1:2 ratio) Composite	Antibiotics (Ciprofloxacin)	Visible Light	97.83% removal in 120 min (99.05% with H_2O_2)	$O_2^{\bullet-}$, $OH^{\bullet}$, h^+	Metallic MXene conductivity suppresses e^-/h^+ recombination.
Cellulose/Ag_2S Composite Film	Organic Dyes (Methylene Blue)	Sunlight / NIR	$33\text{--}35\%$ in dark vs. $> 90\%$ under solar NIR	h^+, $OH^{\bullet}$	Flexible, buoyantly recoverable film; zero secondary sludge.
$SrWO_4$ Bifunctional Material	Emerging Water Pollutants	Visible Light	$98.2\text{--}99.75\%$ pollutant recovery & removal	h^+, $O_2^{\bullet-}$	Dual adsorption and catalytic oxidation functionality.
TiO_2/ g-C_3N_4@Ag Ternary Composite	Nitro-aromatics (4-NP) & Heavy Metals	UV / Solar	$> 95\%$ 4-NP reduction; 80% Cr(VI) reduction	e^-_{CB}, $OH^{\bullet}$	Simultaneous organic degradation and heavy metal reduction.
Green-tea N-gZnOw Nanomaterial	Antibiotics (CIP, CLO, TEM)	UV-Vis	Complete target degradation achieved	$O_2^{\bullet-}$, $OH^{\bullet}$	Eco-friendly green synthesis; optimized zinc hexahydrate precursor.
Electrospun La-TiO_2/PAN Nanofiber Membrane	Pesticides / Micropollutants	LED Light	81.68% efficiency retained after 5 cycles	$OH^{\bullet}$, $O_2^{\bullet-}$	Continuous flow self-cleaning membrane; no particle leaching.

Analysis of these kinetic benchmarks highlights the operational advantages of functionalized nanocomposite systems. Integrating conductive carbon supports (e.g., MXenes, biochar) or plasmonic metal relays (e.g., Ag nanoparticles) into wide-bandgap semiconductors accelerates interfacial charge transport. This spatial charge separation increases the apparent pseudo-first-order rate constant (k) by up to an order of magnitude compared to unfunctionalized base materials (Bogdanović et al., 2025).

Combining photo-oxidation with adsorptive concentration as demonstrated by high-surface-area MOFs like ZnCuCr-TpIm ($\sim 1000\ \text{m}^2 \cdot \text{g}^{-1}$) and biochar-supported composites enhances mass transfer. This spatial proximity allows short-lived reactive oxygen species (such as $OH^{\bullet}$, which has a half-life of $\sim 10^{-9}$ s) to attack target pollutants immediately upon generation, increasing overall mineralization efficiency. In addition, engineering composite materials for near-infrared (NIR) responsiveness (e.g., narrow-bandgap Ag_2S films) expands solar spectrum utilization beyond the UV and visible regions into the NIR regime (> 700 nm), which constitutes nearly half of incoming solar energy (Kutuzova et al., 2021).

© 2026 The Authors. This article is an Open Access article distributed under the terms and conditions of the Creative Commons Attribution(CC–BY)license
https://creativecommons.org/licenses/by/4.0

6. Reactor Design, Immobilization, and Operational Challenges

6.1 Immobilization Strategies and Flow Reactors

Slurry-based photocatalytic reactors suffer from high operational costs due to the complex post-treatment filtration and centrifugation required to recover suspended sub-micron powders. Powder loss can also lead to secondary particulate pollution in discharged effluents. To solve these practical issues, recent engineering efforts focus on immobilizing nanocomposite photocatalysts onto porous, continuous macro-structures (Guan et al., 2025).

Incorporating photocatalytic nanocomposites into electrospun polymer matrices (such as polyacrylonitrile [PAN]) yields flexible, porous catalytic membranes. Advanced electrospinning geometries, such as core-shell configurations, encapsulate the active nanocomposite within a protective porous polymer sheath. This design prevents particle detachment, maintains mechanical strength, and ensures long-term operational stability with over 81% efficiency retained after multiple continuous flow cycles (Giannakoudakis et al., 2022).

Anchoring narrow-bandgap semiconductors onto lightweight, flexible matrices (such as cellulose or biopolymer hydrogels) produces floatable catalytic films. These buoyant materials sit at the air-water interface, maximizing incident solar light interception while eliminating the need for energy-intensive mechanical aeration or slurry pumping (Adewumi et al., 2020).

In parallel, immobilizing heterojunction nanocomposite powders onto fixed substrates (such as glass beads, ceramic monoliths, or stainless-steel meshes) enables continuous-flow water remediation. For example, pilot-scale solar units utilizing immobilized bismuth oxychloride (BiOCl) have achieved over 75% pollutant degradation under natural solar irradiation at operational doses of $100\ \mathrm{kJ \cdot L^{-1}}$, confirming the viability of fixed-bed configurations for practical applications (Jia et al., 2021).

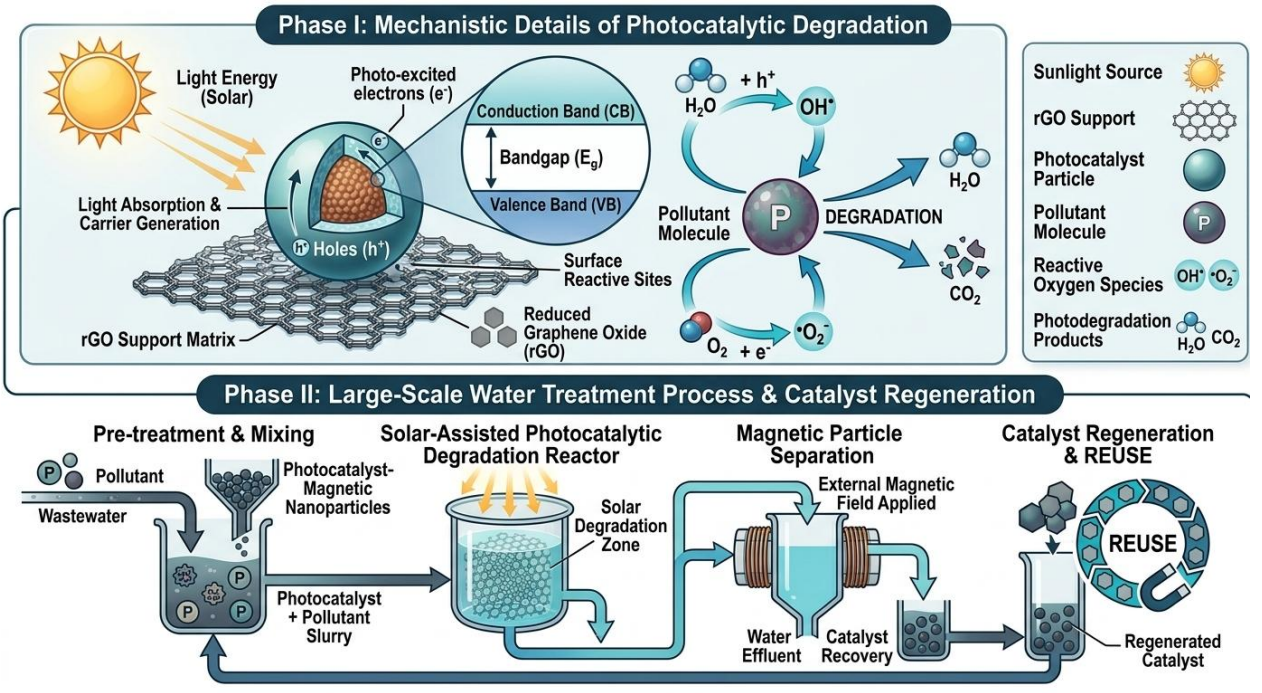


Figure 2: Overview of photocatalytic degradation mechanisms on rGO-supported nanocomposites (Phase I) coupled with a large-scale continuous solar-assisted water treatment reactor and magnetic catalyst regeneration workflow (Phase II).

© 2026 The Authors. This article is an Open Access article distributed under the terms and conditions of the Creative Commons Attribution(CC–BY)license
https://creativecommons.org/licenses/by/4.0

6.2 Catalyst Recovery, Matrix Effects, and Leaching Hazards

Deploying functionalized nanocomposites in real-world wastewater treatment introduces several operational challenges. Slurry-based nanocomposites can be modified by incorporating superparamagnetic magnetite cores (Fe_3O_4) to create magnetically recoverable systems, such as TiO_2/AC/Fe_3O_4 or ZnO-Fe_3O_4. Applying an external magnetic field rapidly isolates the catalyst from treated water, enabling catalyst recovery and reusability over multiple consecutive cycles with minimal loss in performance (Adewumi et al., 2020).

When using metal-organic frameworks (MOFs) or transition-metal-doped oxides, extended exposure to extreme pH levels, high salinity, or natural organic matter (NOM) can induce structural degradation. This dissolution risks leaching toxic transition metal ions (Ni^{2+}, Cr^{3+}, Co^{2+}, Cd^{2+}) or organic linkers into treated water bodies. Evaluating catalyst durability requires testing under realistic aqueous conditions, using analytical techniques such as ICP-OES to verify that metal leaching remains below international drinking water safety thresholds (Ahmed et al., 2017).

Furthermore, actual industrial effluents, landfill leachates, and municipal wastewaters contain complex mixtures of inorganic anions (Cl^-, SO_4^{2-}, HCO_3^-), natural organic matter, and varying turbidity. Inorganic anions act as radical scavengers, consuming $OH^\bullet$ to form weaker secondary inorganic radicals ($Cl^\bullet$, $CO_3^{\bullet-}$), which slows target pollutant degradation rates. Suspended solids and high COD reduce photon penetration through the water column, lowering light availability at the catalyst surface (Samal et al., 2022). Competing organics continuously occupy active surface adsorption sites, reducing overall catalytic throughput. Overcoming these operational challenges requires designing nanocomposite systems with high selectivity, optimizing continuous-flow reactor configurations, and evaluating catalyst performance under multi-pollutant conditions (Richardson & Ternes, 2018).

7. Conclusion

This review has systematically consolidated the fundamental principles, engineering strategies, and mechanistic pathways governing the photocatalytic degradation of emerging organic pollutants using functionalized semiconductor nanocomposites. The thermodynamic framework established through Mulliken electronegativity theory and Nernstian flat-band potential analysis provides a rigorous basis for predicting ROS generation capability, while Langmuir–Hinshelwood kinetics and adsorption isotherm modeling offer quantitative tools for evaluating interfacial degradation performance. The evolution from conventional Type-II heterojunctions to Direct Z-Scheme and S-Scheme architectures represents a critical breakthrough, as these designs overcome the intrinsic redox potential sacrifice of Type-II systems by preserving the most powerful photogenerated electrons and holes for superoxide and hydroxyl radical generation, respectively. Functionalization with carbonaceous matrices particularly biochar and CNTs enhances surface area, pollutant adsorption, and charge conductivity, while MOFs contribute ultrahigh porosity and tunable band edges, albeit with stability concerns under extreme pH and saline conditions. The case studies on ciprofloxacin, PFOA/PFAS, and microplastics demonstrate that tailored nanocomposites can achieve near-complete mineralization through competitive pathways including piperazine ring cleavage, defluorination, and Norrish-type photo-oxidation, with ECOSAR modeling confirming reduced toxicity of transformation intermediates. Performance benchmarking reveals that S-scheme systems such as α-Fe_2O_3/g-C_3N_4 and La/MXene composites achieve superior kinetic rate constants and reusability, while magnetic Fe_3O_4-based composites enable practical catalyst recovery. Nevertheless, significant challenges persist: metal ion leaching from MOFs and doped oxides, radical scavenging by inorganic anions (Cl^-, SO_4^{2-}, HCO_3^-), photon attenuation in turbid effluents, and the lack of standardized pilot-scale validation under real wastewater matrices. Future research must prioritize the development of hydrolytically stable, selective nanocomposites; the integration of continuous-flow immobilized-bed reactors with solar concentrators; and the adoption of unified ecotoxicity and life-cycle assessment protocols. By addressing these gaps, functionalized semiconductor photocatalysis can transition from laboratory promise to a deployable, sustainable technology for safeguarding water quality against the growing threat of emerging organic pollutants.

© 2026 The Authors. This article is an Open Access article distributed under the terms and conditions of the Creative Commons Attribution(CC–BY)license
https://creativecommons.org/licenses/by/4.0

References

[1]. Adeoye, J. B., Tan, Y. H., Lau, S. Y., Tan, Y. Y., Chiong, T., Mubarak, N. M., & Khalid, M. (2024). Advanced oxidation and biological integrated processes for pharmaceutical wastewater treatment: A review. Journal of Environmental Management, 354, Article 120170. https://doi.org/10.1016/j.jenvman.2024.120170

[2]. Adewumi, O. O., Omotola, E. O., & Olatunji, O. S. (2020). Pharmaceuticals and personal care products in water and wastewater: A review of treatment processes and use of photocatalyst immobilized on functionalized carbon in AOP degradation. BMC Chemistry, 14, Article 62. https://doi.org/10.1186/s13065-020-00714-1

[3]. Ahmed, M. B., Zhou, J. L., Ngo, H. H., Guo, W., Thomaidis, N. S., & Xu, J. (2017). Progress in the biological and chemical treatment technologies for emerging contaminant removal from wastewater: A critical review. Journal of Hazardous Materials, 323, 274–298. https://doi.org/10.1016/j.jhazmat.2016.04.045

[4]. Bellucci, S. (2026). Carbon/Inorganic Hybrid Multifunctional Composites: Interface Engineering, Coupled Functions and Application-Ready Design. *Inorganics*, *14*(6), 160.

[5]. Binjhade, R., Mondal, R., & Mondal, S. (2025). Photocatalytic degradation of ciprofloxacin and metformin in a continuous-flow tubular reactor. *Reaction Chemistry & Engineering*, *10*(7), 1577-1586.

[6]. Bogdanović, T., Listeš, I., Gjerde, J., Petričević, S., Jažo, Z., Listeš, E., ... & di Giacinto, F. (2025). Microplastic polymer mass fractions in marine bivalves: From isolation to hazard risk. *Journal of xenobiotics*, *15*(6), 186.

[7]. Choe, M. G., Kang, M. J., & Jang, H. W. (2026). Ferroelectricity-Enhanced Photocatalysis: Mechanisms, Materials, and Engineering Strategies. *Solar RRL*, *10*(6), e202500919.

[8]. Dharsandia, I., Kumar, N., Tiwari, A., Tiwari, B. S., Nagar, M. R., & Mishra, S. K. (2026). Next generation materials for environmental remediation through advanced mechanisms and future perspectives. *Discover Nano*, *21*(1), 408.

[9]. Giannakoudakis, D. A., Zormpa, F. F., Margellou, A. G., Qayyum, A., Colmenares-Quintero, R. F., Len, C., ... & Triantafyllidis, K. S. (2022). Carbon-based nanocatalysts (CnCs) for biomass valorization and hazardous organics remediation. *Nanomaterials*, *12*(10), 1679.

[10]. Gollavelli, G., & Ling, Y. (2025). Shaping Clean Water Futures with Carbon-Based Nanomaterials: A Comprehensive Review.

[11]. Guan, X., Lei, Z., Xue, R., Li, Z., Li, P., David, M., ... & Ma, T. (2025). Polarization: a universal driving force for energy, environment, and electronics. *Advanced Materials*, *37*(1), 2413525.

[12]. Hoffmann, M. R., Martin, S. T., Choi, W., & Bahnemann, D. W. (1995). Environmental applications of semiconductor photocatalysis. Chemical Reviews, 95(1), 69–96. https://doi.org/10.1021/cr00033a004

[13]. Hong, J., Cho, K. H., Presser, V., & Su, X. (2022). Recent advances in wastewater treatment using semiconductor photocatalysts. Current Opinion in Green and Sustainable Chemistry, 36, Article 100644. https://doi.org/10.1016/j.cogsc.2022.100644

[14]. Hossain, M. (2024). Trending physico-chemical characteristics of microplastics (MPs) and nano-plastics (NPs) in different physical environments and their role in various emerging environmental issues: A review. *Available at SSRN 5095223*.

[15]. Hui, K., Song, J., Xi, B., Yuan, Y., & Tan, W. (2026). Generation mechanisms, environmental behaviors, and treatment technologies of conventional and emerging contaminants in landfill leachate: A review. Environmental Chemistry and Ecotoxicology, 319–338. https://doi.org/10.1016/j.enceco.2025.11.030

[16]. Ioni, Y. V., Farooq, M., Roshka, D., Pal, A. K., Krasnikov, D. V., & Nasibulin, A. G. (2025). Microplastic generation, distribution, and removal from the environment: a review. *Russ. Chem. Rev*, *94*(3).

[17]. Jia, Z., Lv, R., Guo, L., Zhang, J., Li, R., Liu, J., & Fan, C. (2021). Rapid degradation of ciprofloxacin over BiOCl: Insight into the molecular structure transformation and antibacterial activity elimination. *Separation and Purification Technology*, *257*, 117872.

[18]. Johannessen, C., & Shetranjiwalla, S. (2021). Role of structural morphology of commodity polymers in microplastics and nanoplastics formation: Fragmentation, effects and associated toxicity in the aquatic environment. *Reviews of Environmental Contamination and Toxicology Volume 259*, 123-169.

[19]. Kjeldsen, P., Barlaz, M. A., Rooker, A. P., Baun, A., Ledin, A., & Christensen, T. H. (2002). Present and long-term composition of MSW landfill leachate: A review. Critical Reviews in Environmental Science and Technology, 32(4), 297–336. https://doi.org/10.1080/10643380290813462

[20]. Kumar, P., Thakur, N., Kaur, J., Kaur, P., & Rahul. (2026). Carbon-Based Nanocomposite for Environmental Catalysis. In *Carbon-Based Nanocomposites for Sustainable Applications, Volume III: Biomedicine, Electronics, and Catalysis* (pp. 341-364). Cham: Springer Nature Switzerland.

[21]. Kümmerer, K. (2009). Antibiotics in the aquatic environment A review Part I. Chemosphere, 75(4), 417–434. https://doi.org/10.1016/j.chemosphere.2008.11.086

[22]. Kutuzova, A., Dontsova, T., & Kwapinski, W. (2021). Application of TiO2-based photocatalysts to antibiotics degradation: cases of sulfamethoxazole, trimethoprim and ciprofloxacin. *Catalysts*, *11*(6), 728.

[23]. Liao, M., Zhao, S., Zhan, G., Liang, J., Li, Z., Dong, F., ... & Zhang, L. (2025). Silicate-confined hydrogen on nanoscale zerovalent iron for efficient defluorination reactions. *Journal of the American Chemical Society*, *147*(4), 3402-3411.

[24]. Mehmood, N., Rajput, V. D., Mazhar, S., Hyder, S., Banerjee, S., Gedefaw, M., ... & Minkina, T. (2026). PFAS in soil systems: rethinking microbial responses, methodological biases and emerging risks. *Environmental Pollutants and Bioavailability*, *38*(1), 2706235.

[25]. Mukherjee, I., Cilamkoti, V., & Dutta, R. K. (2021). Sunlight-driven photocatalytic degradation of ciprofloxacin by carbon dots embedded in ZnO nanostructures. *ACS Applied Nano Materials*, *4*(8), 7686-7697.

© 2026 The Authors. This article is an Open Access article distributed under the terms and conditions of the Creative Commons Attribution(CC–BY)license
https://creativecommons.org/licenses/by/4.0

[26]. Richardson, S. D., & Ternes, T. A. (2018). Water analysis: Emerging contaminants and current issues. Analytical Chemistry, 90(1), 398–428. https://doi.org/10.1021/acs.analchem.7b04577

[27]. Rout, P. R., Zhang, T. C., Bhunia, P., & Surampalli, R. Y. (2021). Treatment technologies for emerging contaminants in wastewater treatment plants: A review. Science of the Total Environment, 753, Article 141990. https://doi.org/10.1016/j.scitotenv.2020.141990

[28]. Samal, K., Mahapatra, S., & Ali, M. H. (2022). Pharmaceutical wastewater as emerging contaminants (EC): Treatment technologies, impact on environment and human health. Energy Nexus, 6, Article 100076. https://doi.org/10.1016/j.nexus.2022.100076

[29]. Sayed, M., Zhang, L., Garcia, H., Yu, H., & Yu, J. (2026). S-scheme shapes heterojunction photocatalysis. *Accounts of Chemical Research*, *59*(7), 1138-1153.

[30]. Schneider, J., Matsuoka, M., Takeuchi, M., Zhang, J., Horiuchi, Y., Anpo, M., & Bahnemann, D. W. (2014). Understanding TiO_2 photocatalysis: Mechanisms and materials. Chemical Reviews, 114(19), 9919–9986. https://doi.org/10.1021/cr5001892

[31]. Singh, H., Dhanu, A. S., Joshi, A. S., Mijakovic, I., & Singh, P. (2026). Next-generation nanomaterials for environmental remediation: smart design, hybrid materials and sustainable use. *Frontiers in Chemistry*, *14*, 1772161.

[32]. Soleimani, M., & Pacchioni, G. (2025). Effect of W–Mo Composition on the Interfacial Electronic Structure and Photoelectrochemical Performance of CuW1–x Mo x O4/BiVO4 Heterojunctions. *ACS Applied Energy Materials*, *8*(15), 11570-11583.

[33]. Wan, X. Y., Zhao, Y., Wen, H. Z., Zhang, H. T., Wan-Mo, Z. X., Xie, Y. L., & Pan, L. (2025). Synergistic activation of MgFe2O4/ZnO photocatalyst with peroxymonosulfate enables efficient degradation of ciprofloxacin: a study on radical multipath mechanisms. *Colloids and Surfaces A: Physicochemical and Engineering Aspects*, 138968.

[34]. Wang, Y., Ji, S., & Shin, B. (2022). Interface engineering of antimony selenide solar cells: a review on the optimization of energy band alignments. *Journal of Physics: Energy*, *4*(4), 044002.

[35]. Wright, S. L., & Kelly, F. J. (2017). Plastic and human health: A micro issue? Environmental Science & Technology, 51(12), 6634–6647. https://doi.org/10.1021/acs.est.7b00423

[36]. Wu, H., Li, L., Wang, S., Zhu, N., Li, Z., Zhao, L., & Wang, Y. (2023). Recent advances of semiconductor photocatalysis for water pollutant treatment: Mechanisms, materials and applications. Physical Chemistry Chemical Physics, 25, 25899–25924. https://doi.org/10.1039/D3CP03391K

[37]. Yang, L., Hu, T., Zhang, D., Zhou, W., & Lin, D. (2026). Broad-spectrum defluorination via electronic strain of carbon–fluorine bonds: a'fluorophilic'zero-valent metal system. *Water Research*, 126495.

[38]. Yao, M., Liu, Y., Zhang, L., Wang, J., Xu, C., Qian, T., & Liu, X. (2025). Synergistic adsorption and photodegradation of ciprofloxacin in water by biochar-supported titanates: mechanistic analysis, DFT calculations and toxicity risk assessment. *Journal of Water Process Engineering*, *70*, 106964.

© 2026 The Authors. This article is an Open Access article distributed under the terms and conditions of the Creative Commons Attribution(CC–BY)license
https://creativecommons.org/licenses/by/4.0